Hindawi Publishing Corporation
Journal of Photonics
Volume 2014, Article ID 309350, 6 pages
http://dx.doi.org/10.1155/2014/309350

Research Article

Graphene Embedded Modulator with Extremely Small Footprint and High Modulation Efficiency

Ran Hao and Jia-Min Jin

Department of Information Science & Electronic Engineering, Radio Frequency & Nano-Electronic Research Centre, Zhejiang University, Hangzhou 310027, China

Correspondence should be addressed to Ran Hao; rhao@zju.edu.cn

Received 11 February 2014; Revised 8 May 2014; Accepted 8 May 2014; Published 28 May 2014

Academic Editor: Anatole Lupu

By embedding graphene sheet in the silicon waveguide, the overall effective mode index displays unexpected symmetry and the electrorefraction effect has been significantly enhanced near the epsilon-near-zero point. An eight-layer graphene embedded Mach-Zehnder Modulator has been theoretically demonstrated with the advantage of ultracompact footprint ($4 \times 2\,\mu m^2$), high modulation efficiency ($1.316\,V{\cdot}\mu m$), ultrafast modulation speed, and large extinction ratio. Our results may promote various on-chip active components, boosting the utilization of graphene in optical applications.

1. Introduction

Electrooptical modulator, which transfers electronic signals into high bit-rate photonic data, is the key component in on-chip interconnection and integrated optoelectronic circuits [1]. By applying an electric field to a material, the real and imaginary part of the refractive indices can be changed. A change in the real part of the refractive index caused by the applied voltage is known as the electrorefraction (ER) effect, whereas a change in the imaginary part of the refractive index is known as the electroabsorption (EA) effect [1]. However, these two effects are too weak in pure silicon at the communication wavelengths so that it usually needs an extremely large length to reach the required modulation; for example, a 50 Gbit/s modulator has the length of 1 millimeter [2]. The large footprint of optical modulator makes it impossible to be integrated into a single chip. To fill the demands of next generation on-chip communication, minimizing the size and improving the speed of modulator become the urgent goals but remain a challenge. Recently, graphene-based modulators have attracted much attention due to their unprecedented ability to enhance the material's EA effect; thus, they can greatly reduce the modulator length to achieve the same effect [2–5]. In [5], Lu and Zhao reported a graphene embedded modulator having a length of only 1 μm. However, limited by the inbuilt drawback from the EA modulator, the extinction ratio is low and background noise cannot be ignored.

In this paper, we point out that graphene can also have significant enhancement to the ER effect of the background material. By embedding duplicated graphene layers into a silicon substrate, we demonstrated that the variation of effective mode index Δn_{eff} can be as large as 0.4057 corresponding to a Mach-Zender modulation arm length of only 1.9 μm. Note that Δn_{eff} caused by ER effect is only at the level of 10^{-4} for conventional semiconductor modulators [6–8]. To our knowledge, this is the largest Δn_{eff} and smallest modulation arm length ever reported. In addition, our proposed ER modulator has the advantage of large bandwidth, high modulation speed, large extinction ratio, as well as low noise.

2. The Symmetry of Refractive Index

Graphene is a single atom thick two-dimensional carbon sheet, whose permittivity can be actively tuned by the chemical potentials (the Fermi level). Figure 1 shows the permittivity ε of an infinite graphene sheet obtained from the Kubo formula [9] at the wavelength $\lambda = 1550$ nm (corresponding photon energy $\hbar\omega = 0.802$ eV). It can be seen that there is a dip in the curve of permittivity magnitude,

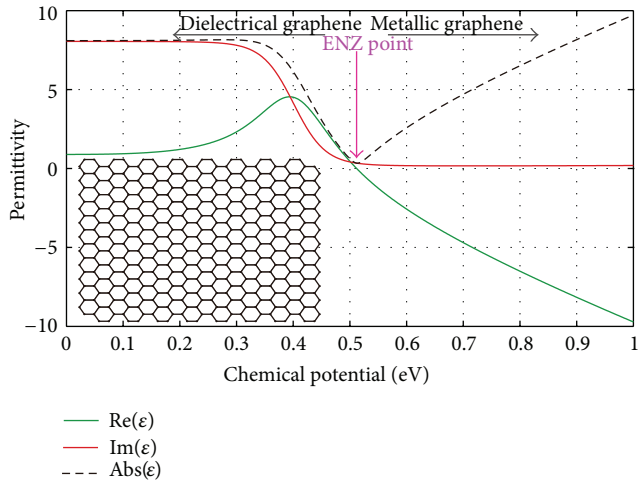

FIGURE 1: The permittivity of an infinite graphene sheet: the green/red/black-dot curve indicates the real part/imaginary part and the absolute value of permittivity. The inset picture indicates an infinite graphene sheet. The chemical potential varies from 0 to 1 eV, and the wavelength is fixed at 1550 nm.

and the epsilon-near-zero (ENZ) point is obtained at the chemical potential $\mu_{C0} = 0.513$ eV where the absolute value of epsilon is approaching zero. When the chemical potential $\mu_C < \mu_{C0}$, both the real and imaginary part of the permittivity (Re(ε) and Im(ε)) have the positive sign so that the graphene layer behaves like a dielectric material. When $\mu_C > 0.52$ eV, Re(ε) becomes negative and Im(ε) is approaching zero, this means that the graphene sheet acts like a metallic layer, and it is then fabulous to transfer surface plasmons [10]. When the chemical potential is gradually increased, the "dielectric graphene" is gradually transforming into "metallic graphene" at the ENZ point $\mu_{C0} = 0.513$ eV; therefore, it can be called as the transition chemical potential. It should be noted that there exists a range (0.48 eV $< \mu < 0.52$ eV), where both Re(ε) and Im(ε) are very close to zero so that the ENZ effect appears, and the graphene layer exhibits unexpected new properties [11, 12], propelling various active optoelectronic devices [12]. Moreover, we have checked the performance of the entire telecom-band (C/L/O/E-band), and it turns out that the ENZ point exists at each telecom band. We choose the particular wavelength around 1550 nm, because it is a region of low loss for optical fibers and therefore of interest for optical communication systems. In the following, we will focus on this special area to configure an optical modulator.

To enhance the graphene-light interaction, the structure with the graphene layer embedded in the center of the silicon waveguide is considered since the rectangle waveguide tends to concentrate light in the center. By applying a drive voltage upon the waveguide, the chemical potential of the graphene layer can be modified, which in turn affects the permittivity of graphene layer. Therefore, the permittivity of the overall waveguide will be influenced, and the effective modal index (n_{eff}) of the whole waveguide will be also changed. From the previous analysis, it is shown that there is a special ENZ point at $\mu_{C0} = 0.513$ eV, where the "epsilon-near-zero" effect takes place (both Re(ε) and Im(ε) of graphene are approaching zero). In Figure 2, the real and imaginary part of effective mode index for the proposed waveguide in the ENZ area are investigated through the rigorous mode analysis from finite element package COMSOL. When μ_C is close to μ_{C0}, the n_{eff} does change drastically as expected, inferring the corresponding mode properties that change a lot when the embedded graphene layer transfers from its dielectric state to metallic state. Furthermore, for such silicon-graphene-silicon waveguide, both Re(ε) and Im(ε) have unexpected symmetries towards the ENZ point. As depicted in Figures 2(a)–2(c), Re(ε) displays an odd-symmetry towards the ENZ point, while Im(ε) displays an even-symmetry. As the Im(ε) refers to the propagation loss, the waveguide is expected to have the largest loss at the ENZ point, while there is less propagation loss at the edge side of the curve. The strong variation of loss suggests the chance to build EA modulator, as already reported in [5]. However, the properties of odd-symmetry curve for Re(ε) have been barely explored before. There is a significant increase of Re(ε) in the ENZ area. The variation amount for Re(ε) can be as large as 0.81 for eight layers of graphene embedded waveguide in Figure 2(a). Please note that for doped silicon, the Δn_{eff} is very weak (at the level of 10^{-4}) [6–8]. This means the weak ER effect has been improved by 3 orders of magnitude after multilayer graphene sheets are embedded in the silicon waveguide. The impressive value of large n_{eff} variation is greatly appreciated for the modulators based on ER effect, such as Mach-Zehnder modulator. It can be inferred that the number of graphene layers does not influence the scope of the even and odd symmetry distribution, but can affect the Δn_{eff} amount. The more the numbers of graphene layers there are, the more the enhancements that can be produced and the larger the index variation that can be observed.

3. The Mach-Zehnder Modulator

3.1. The Modulator Configuration. To configure a MZI modulator, two pairs of modes (modes A and D and modes B and C) are chosen in Figure 2(a) due to their large Δn_{eff} while maintain roughly the same loss. Modes B and C refer to the largest Δn_{eff}, but the propagation losses of the two modes are 16.37 dB/μm and 14.24 dB/μm following the equation $\alpha = 8.86 * \text{Im}(n_{\text{eff}})$, which are larger than the maximum allowed loss (corresponding to the energy decay to $1/e$ of its initial value, which will be discussed later). Modes A and D have the relatively large $\Delta n_{\text{eff}} = 0.4057$ but simultaneously have relatively low losses. The losses for modes A and D are 2.24 dB/μm and 2.19 dB/μm, respectively, which are smaller than the maximum allowed loss.

The normalized electric field distribution for mode A is depicted in Figure 2(b) in 2D form and also in Figure 2(d) in 3D form. In Figure 2(d), there is a Gaussian-like field distribution inside the waveguide—the maximum fields are achieved in the center of the waveguide but decay exponentially away from the center, while the minimum fields are at the edges of the waveguide. One important feature is that the fields in the graphene layers are much stronger

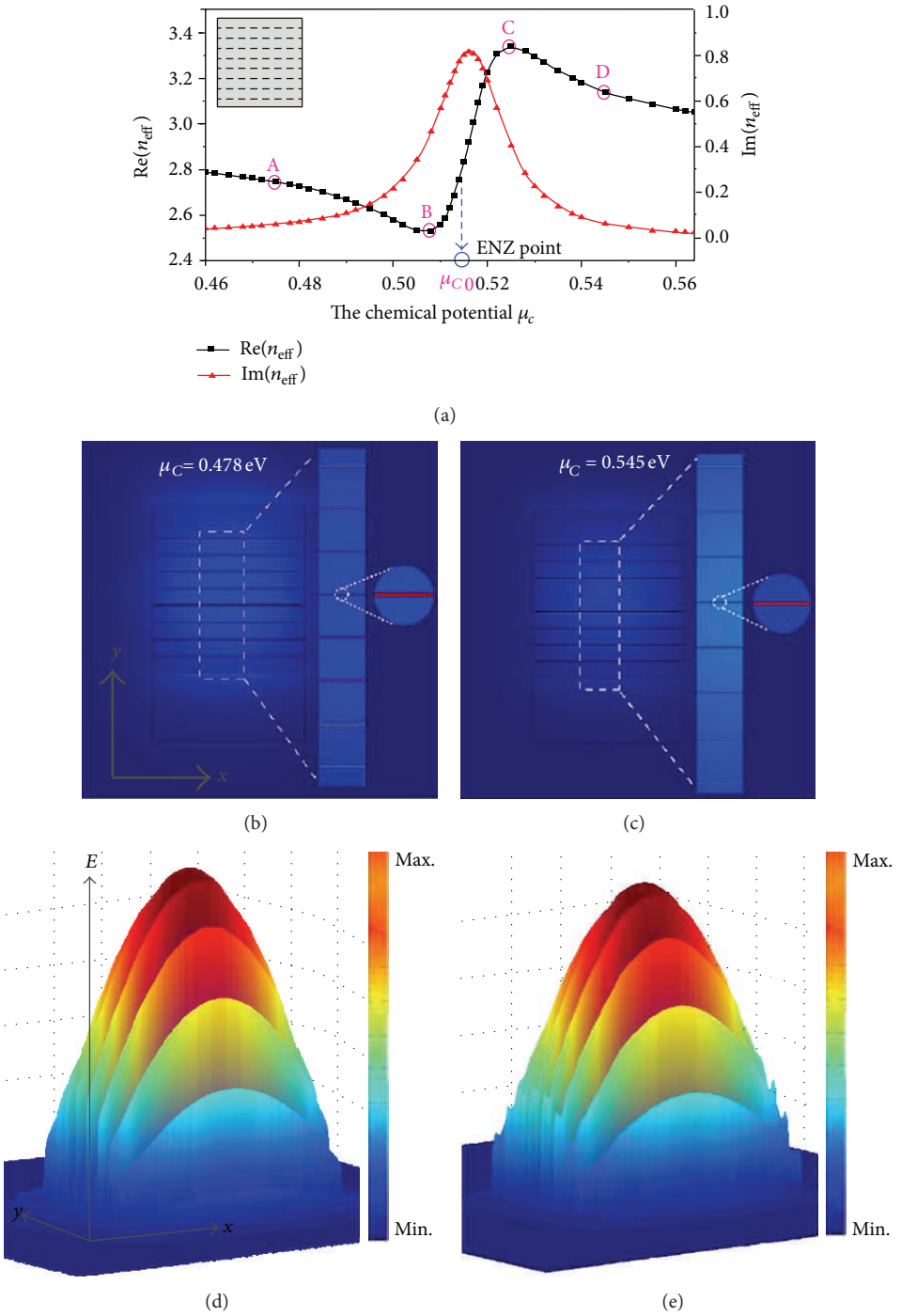

FIGURE 2: The real and imaginary part of effective modal index variation under different chemical potentials for graphene-embedded waveguide: (a) silicon waveguide with one layer graphene embedded, (b) silicon waveguide with two-layer graphene embedded, and (c) silicon waveguide with eight-layer graphene embedded. The insert pictures in (a), (b), and (c) show the schematics for waveguide structures. μ_{C0} = 0.513 eV corresponds to the epsilon-near-zero point. The insert pictures of (d) and (e) are the 3D distribution of E field-intensity of μ_{C0} = 0.513 eV which corresponds to the ENZ point.

than the fields in the background, as depicted in the insert of Figure 2(b). This is because the refractive index for the graphene layer at μ_C = 0.478 eV is 1.207, which is smaller than the index of background silicon (n = 3.45). Therefore, the silicon-graphene-silicon configuration forms a nanoscale slot waveguide that the magnitude of the electric field is much larger in the low index media [13]. On the other hand, Figures 2(c) and 2(e) show the normalized electric field distribution for mode D in 2D and 3D forms, respectively. In Figure 2(e), it can be seen that the fields are not only

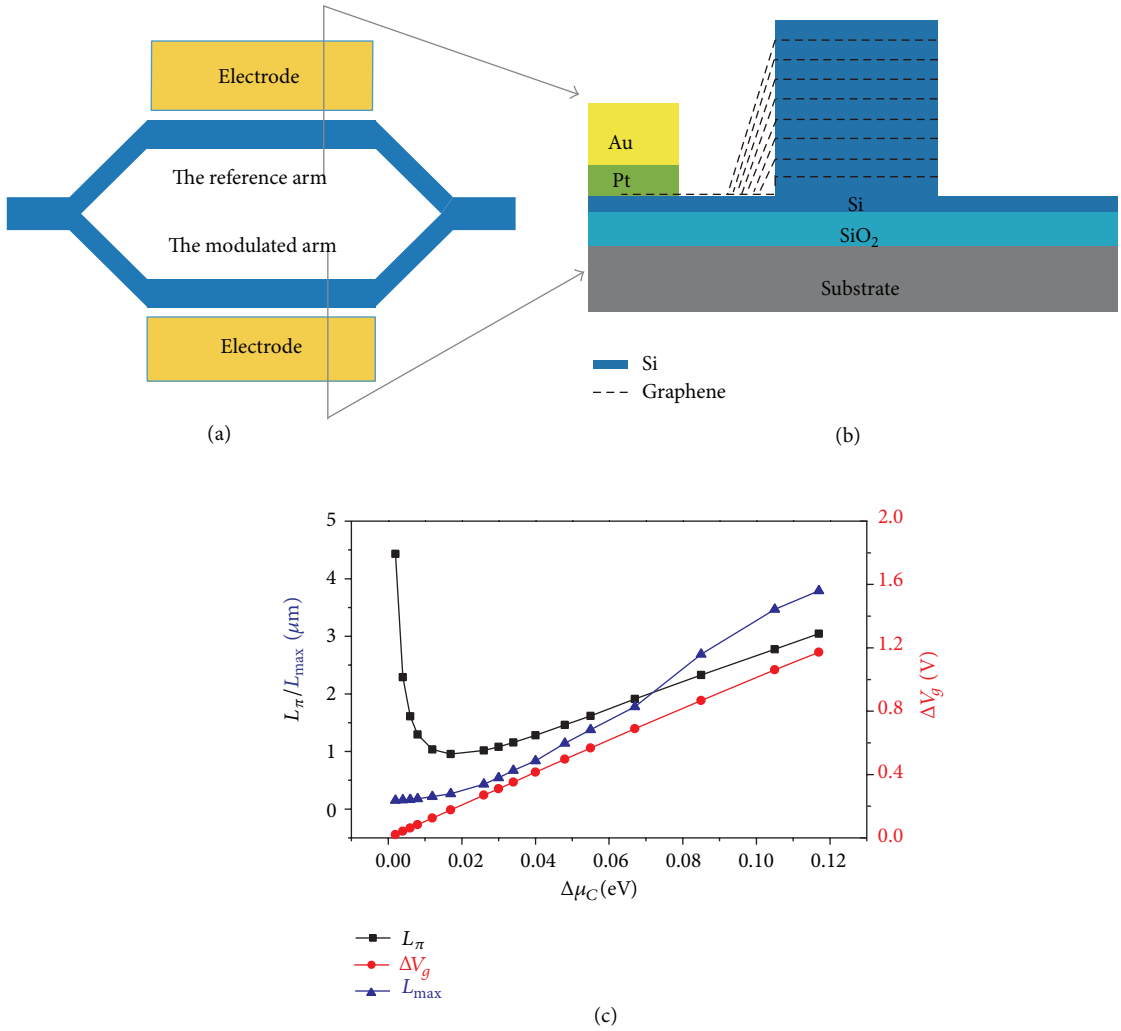

FIGURE 3: The schematic picture of the MZI modulator is shown in (a) and (b). (c), the permittivity of an infinite graphene sheet: the green/red/black-dot curves indicate the real part/imaginary part, and the absolute value of permittivity. The inset picture indicates an infinite graphene sheet. The chemical potential varies from 0 to 1 eV, and the wavelength is fixed at 1550 nm.

concentrate in the center but also appear at the edges of the waveguide. Moreover, when $\mu_C = 0.545$ eV, the epsilon of graphene layer is −1.102, where the graphene layer starts to behave like a metallic layer. Therefore, the edge effect appears and the corresponding mode is quite strong at the edge of the waveguide which is the sign of Surface Plasmon Polariton (SPP) mode [14]. In short summary, the proposed 8-layer graphene waveguide has two operation states. When the chemical potential is smaller than the ENZ point, light is mostly confined inside the graphene layers, and the whole waveguide is a multislot waveguide which has a hybrid dielectric mode. This kind of modes propagates relatively fast, thus it has relatively lower index. When the chemical potential is larger than μ_{C0}, light is concentrated in the center and edge of the waveguide and the whole waveguide has a multihybrid SPP mode. This kind of SPP mode propagates relatively slow, and thus the corresponding mode index is larger. By controlling our waveguide shifts between these two kinds of modes, a large index difference as large as 0.4057 can be produced.

3.2. Figure of Merits. The schematic picture for the proposed MZI modulator is shown in Figures 3(a) and 3(b). In practice, the graphene sheet can be grown in CVD, and transferred on the silicon-on-insulator substrate. The modulation arm has the width of 450 nm, and the distance between the two arms is 1.1 μm. To maintain the large Δn_{eff}, the chemical potentials μ_C of the two operation states can be chosen according to the ENZ point: one should be smaller than the transition chemical potential (corresponding to the ENZ point), whereas the other should be larger than the transition chemical potential. These two μ_C should have roughly the same interval distance d to the transition chemical potential μ_{C0}. Figure 3(c) investigates the influence of the interval distance between the two chemical potentials ($\Delta\mu_C = 2d$)

to the modulator performance. The critical applied voltage $V_g - V_{\text{Dirac}}$ can be obtained through the following:

$$\mu_C = \hbar V_F \sqrt{\eta\pi \left|\left(V_g - V_{\text{Dirac}}\right)\right|}, \quad (1)$$

where $V_F = 0.9 \times 10^6$ m/s is the Fermi velocity and $\eta = 9 \times 10^{16}$ m^{-2} V^{-1} is estimated from a single capacitor model. Since the voltage offset caused by natural doping V_{Dirac} is a finite number (e.g., 0.8 V in [3]), $V_g - V_{\text{Dirac}}$ can be considered as the applied voltage for simplicity [15]. V_π is the applied voltage to achieve π phase shift which is proportional with the interval distance $\Delta\mu_C$. The arm length to achieve π phase shift can be calculated through $\pi = \Delta n_{\text{eff}} \times L_\pi$ which first decreases then increases as $\Delta\mu_C$ increases. There is an inflection point at $\Delta\mu_C = 0.02$, where L_π and V_π achieve minimum. This situation corresponds to the points B and C in Figure 2(a). As explained before, points B and C correspond to the largest loss, and thus cannot be taken here. The information of propagation loss can be evaluated by the maximum allowed length $L_{\max}$, indicating the length where the energy decays to $1/e$ of its original value. The information of $L_{\max}$ is also plotted in Figure 3(c), showing a cross point with the L_π curve at $\Delta\mu_C = 0.067$. We would focus our attention on the condition that $L_\pi < L_{\max}$ in which case the waveguide has enough power at the output. Under this condition, the highest modulation efficiency $V_\pi L_\pi$ would be achieved at the cross point $\Delta\mu_C = 0.067$ that require smallest L_π and V_π to achieve π phase shift. Let us now consider μ_{C1} =0.478 eV for the "on" state and $\mu_{C2} = 0.545$ eV for the "off" state; these two points have relatively low loss but a large Δn_{eff} at 0.4057. Thus the arm length of a MZI modulator to achieve a π phase shift is only 1.9 μm according to $\Delta\varphi = \Delta n_{\text{eff}} \times L$, which is three orders of magnitude smaller than the present reported value [6–8]. The corresponding required applied voltages should be 2.3 V for the "on" state and 3.0 V for the "off" state, indicating a small tuning voltage V_π of 0.7 V. The modulation efficiency is thus 1.316 V·μm, which is much smaller if compared with recent value in [16]. Furthermore, taking into account of the electrode width of 1 μm on each arm side, the overall width of the device is 4 μm, and thus the footprint of our proposed modulator is only $4 \times 2\,\mu\text{m}^2$, which is smaller if compared with recent phase modulator [15]. This smallest size as well as the CMOS compactable structure indicates its valuable capability to be integrated into photonic circuits in a single chip.

The modulation bandwidth is usually characterized by the cutoff frequency (or the 3 dB bandwidth) which is defined by the frequency when the modulation is reduced to 50% of its maximum value. Unlike the semiconductor modulator which has speed limitation posed by the minority carrier lifetime, the graphene modulator has no carrier limitation. Therefore, it can be simply evaluated by the RC delay $f_{3\,\text{dB}} = 1/2\pi\text{RC}$, where the effective resistance is 5 Ω and the effective capacitance is 128 fF. Thus, the predicted modulation bandwidth of our eight-layer graphene modulator is 250 GHz. It should be noted that the most recent reported bandwidth of pure silicon modulator is only 50 GHz [15] and the limitation of silicon is 485 GHz [17]. Also, the modulation speed is estimated at about 500 Gbit/s through the expression $B = 2$ W (binary element).

One significant advantage for MZI modulator is that the extinction ratio is large if compared with other modulators [18]. In principle, the π phase shift between two arms in MZI modulator leads to absolute "0" output for the "off" state. The absolute "0" output requires the light pulses in the two arms to have the exact same intensity but the opposite sign. These requirements can be satisfied in our modulator; due to the even symmetry for Im(ε), propagation loss in two arm can be equal, thus light intensities are equal to each other; while the phase different between the two arms $\Delta\varphi = \Delta n_{\text{eff}} \times L$ can be designed to π as long as we take appropriate L_π, indicating light at the two arms have opposite signs. Even at the unoptimized situation for points A and D in Figure 2(c) with $\mu_{C1} = 0.478$ eV and $\mu_{C2} = 0.545$ eV, the extinction ratio still can reach 19.64 dB. We should mention that a much higher extinction ratio can be achieved as long as μ_{C1} and μ_{C2} are chosen with exactly the same Im(n_{eff}).

In conclusion, by embedding graphene sheet into the silicon waveguide, the Re(n_{eff}) and Im(n_{eff}) display unexpected symmetries towards the ENZ point and the ER effect has been significantly enhanced near the ENZ point. An eight-layer graphene sheets embedded modulator has been proposed based on this effect, with the advantage of ultracompact footprint ($2 \times 4\,\mu\text{m}^2$), extremely short arm length (1.9 μm), low drive voltage (3 V), high modulation efficiency (1.316 V·μm), large modulation bandwidth (250 GHz), as well as high extinction ratio. The proposed graphene modulator has great potentials for future active components, showing significant influence for optical interconnects in future integrated optoelectronic systems. The flexibility of graphene sheets may enable radically different photonic devices. The high modulation efficiency as well as ultrafast speed modulation suggests the valuable perspective for utilizing graphene optics in nanophotonic circuits.

Conflict of Interests

The authors declare that there is no conflict of interests regarding the publication of this paper.

Acknowledgments

This work was supported by the National Natural Science Foundation of China (61205054), the Zhejiang Provincial Natural Science Foundation of China (Z1110330 and LQ12F05006), and the Excellent Young Faculty Awards Program (Zijin Plan) at Zhejiang University. The authors would like to thank the helpful discussion with Professor Hongshen Chen and Professor Longzhi Yang at Zhejiang University.

References

[1] G. T. Reed, G. Mashanovich, F. Y. Gardes, and D. J. Thomson, "Silicon optical modulators," *Nature Photonics*, vol. 4, no. 8, pp. 518–526, 2010.

[2] D. J. Thomson, F. Y. Gardes, J. M. Fedeli et al., "50-Gb/s silicon optical modulator," *IEEE Photonics Technology Letters*, vol. 24, no. 4, pp. 234–236, 2012.

[3] M. Liu, X. Yin, E. Ulin-Avila et al., "A graphene-based broadband optical modulator," *Nature*, vol. 474, no. 7349, pp. 64–67, 2011.

[4] M. Liu, X. Yin, and X. Zhang, "Double-layer graphene optical modulator," *Nano Letters*, vol. 12, no. 3, pp. 1482–1485, 2012.

[5] Z. Lu and W. Zhao, "Nanoscale electro-optic modulators based on graphene-slot waveguides," *Journal of the Optical Society of America B*, vol. 29, no. 6, pp. 1490–1495, 2012.

[6] J. H. Wulbern, J. Hampe, A. Petrov et al., "Electro-optic modulation in slotted resonant photonic crystal heterostructures ," *Applied Physics Letters*, vol. 94, no. 24, Article ID 241107, 2009.

[7] D. J. Thomson, F. Y. Gardes, Y. Hu et al., "High contrast 40Gbit/s optical modulation in silicon," *Optics Express*, vol. 19, no. 12, pp. 11507–11516, 2011.

[8] S. J. Spector, M. Geis, G. R. Zhou et al., "CMOS-compatible dual-output silicon modulator for analog signal processing," *Optics Express*, vol. 16, no. 15, pp. 11027–11031, 2008.

[9] G. W. Hanson, "Dyadic Green's functions and guided surface waves for a surface conductivity model of graphene," *Journal of Applied Physics*, vol. 103, no. 6, Article ID 064302, 2008.

[10] A. Vakil and N. Engheta, "Transformation optics using graphene," *Science*, vol. 332, no. 6035, pp. 1291–1294, 2011.

[11] L. Sun and K. W. Yu, "Strategy for designing broadband epsilon-near-zero metamaterial with loss compensation by gain media," *Applied Physics Letters*, vol. 100, no. 26, Article ID 261903, 2012.

[12] S. Vassant, A. Archambault, F. Marquier et al., "Epsilon-near-zero mode for active optoelectronic devices," *Physical Review Letters*, vol. 109, no. 23, Article ID 237401, 2012.

[13] Q. Xu, V. R. Almeida, R. R. Panepucci, and M. Lipson, "Experimental demonstration of guiding and confining light in nanometer-size low-refractive-index material," *Optics Letters*, vol. 29, no. 14, pp. 1626–1628, 2004.

[14] A. Y. Nikitin, F. Guinea, F. J. Garcia-Vidai, and L. Martin-Moreno, "Edge and waveguide terahertz surface plasmon modes in graphene microribbons," *Physical Review B*, vol. 84, Article ID 161407, 2011.

[15] C. Xu, Y. Jin, L. Yang, J. Yang, and X. Jiang, "Characteristics of electro-refractive modulating based on Graphene-Oxide-Silicon waveguide," *Optics Express*, vol. 20, no. 20, pp. 22398–22405, 2012.

[16] X. Xiao, H. Xu, X. Li et al., "High-speed, low-loss silicon Mach-Zehnder modulators with doping optimization," *Optics Express*, vol. 21, no. 4, pp. 4116–4125, 2013.

[17] K. Kim, J. Y. Choi, T. Kim, S. H. Cho, and H. J. Chung, "A role for graphene in silicon-based semiconductor devices," *Nature*, vol. 479, no. 7373, pp. 338–344, 2011.

[18] J. Gosciniak and D. Tan, "Theoretical investigation of graphene-based photonic modulators," *Scientific Reports*, vol. 3, article 1897, 2013.